Research Square

Preprints are preliminary reports that have not undergone peer review.
They should not be considered conclusive, used to inform clinical practice,
or referenced by the media as validated information.

Aβ42 oligomers disrupt calcium homeostasis via Piezo1 and induce neurotoxicity in differentiated SH-SY5Y cells

Weiqi Meng

mwq15244775817@163.com

Changchun Institute of Applied Chemistry

Junye Zhang

Changchun Institute of Applied Chemistry

Shuming Zhang

Changchun University of Technology

Yan Shi

Changchun Institute of Applied Chemistry

Hongda Wang

Changchun Institute of Applied Chemistry

Article

Keywords: Aβ42 oligomers, Piezo1, Calcium homeostasis, Alzheimer's disease, Atomic force microscopy

Posted Date: October 29th, 2026

DOI: https://doi.org/10.21203/rs.3.rs-11212419/v1

License: This work is licensed under a Creative Commons Attribution 4.0 International License.
Read Full License

Additional Declarations: No competing interests reported.

Abstract

Alzheimer's disease (AD) exhibits an intricate and multifactorial pathogenesis. Existing research on amyloid-β (Aβ)-triggered neurotoxicity has predominantly centered on neuronal apoptosis, oxidative stress, and mitochondrial damage. The role of biomechanical signaling, a vital regulatory mechanism in neuronal physiological homeostasis and AD pathological progression, remains largely uncharacterized in the context of Aβ-mediated neurotoxicity. Here, differentiated SH-SY5Y, neuron-like cells, were used to examine the Aβ42 oligomers induced cellular mechanics alteration and the abnormal activation of mechanosensitive ion channels. Aβ42 oligomer adsorption increases cellular Young's modulus, which is associated with sustained intracellular Ca^{2+} elevation mediated by Piezo1. Subsequently, the overloaded Ca^{2+} induces mitochondrial dysfunction, excessive reactive oxygen species accumulation, YAP/TAZ signaling activation, cytoskeletal remodeling, dynamic changes in cellular stiffness, and finally a cell death through caspase-4-mediated non-canonical pyroptosis. These findings support an Aβ42-Piezo1-Ca^{2+}-cytoskeletal remodeling axis that links altered neuronal mechanics to neurotoxicity and identify Piezo1 as a potential target for further investigation in AD.

1. Introduction

Alzheimer's disease (AD) is a progressive neurodegenerative disorder characterized by cognitive decline and behavioral impairment. It is the most common cause of dementia in older adults, accounting for approximately 60–70% of cases, and its incidence increases with age. The principal neuropathological features of AD are extracellular senile plaques composed of amyloid-β (Aβ) [1] and intracellular neurofibrillary tangles containing hyperphosphorylated tau [2]. Aβ42 oligomers are particularly neurotoxic and induce apoptosis in SH-SY5Y cells, a widely used *in vitro* model of AD-related neuronal injury. This response is accompanied by loss of mitochondrial membrane potential, accumulation of reactive oxygen species (ROS), and caspase-3 activation [3, 4]. Aβ42 oligomer treatment also increases oxidative-stress markers, including malondialdehyde, while reducing antioxidant defenses such as superoxide dismutase 1 [5, 6].

In AD, Aβ42 oligomers promote tau hyperphosphorylation, microtubule destabilization, and impaired axonal transport, thereby contributing to synaptic dysfunction [7]. They also disrupt the actin cytoskeleton by inducing abnormal F-actin polymerization and pathological actin aggregates that impair synaptic plasticity [8]. This cytoskeletal reorganization can alter membrane tension, ion-channel activity, mechanochemical signaling, and finally affect cellular Young's modulus. Increased neuronal stiffness has been reported in AD-related models, suggesting a feedback loop between cytoskeletal remodeling and signal transduction [9]. However, the molecular pathway linking Aβ42 oligomers, altered cellular mechanics, and neurotoxicity remains incompletely understood.

Aβ42 oligomers may also influence cell function by altering the mechanical properties of the extracellular matrix [10], raising the possibility that mechanotransduction contributes to AD pathology. Piezo1 is a trimeric mechanosensitive cation channel [11] that responds to membrane tension and

mediates Ca^{2+} influx [12]. Its activity depends strongly on membrane curvature and the mechanical properties of the lipid bilayer [13]. In the nervous system, Piezo1 contributes to calcium-dependent processes, including synaptic plasticity, learning, and memory [14], but its effects vary among cell types. In microglia, Piezo1 senses the stiffness of Aβ fibrils and promotes plaque-associated aggregation, phagocytosis, and compaction [15]; increasing Piezo1 activity can also enhance microglial survival, lysosomal activity, and Aβ clearance [16]. By contrast, Piezo1 activation in neurons and SH-SY5Y cells exposed to Aβ has been associated with mitochondrial depolarization and cell death [6, 17].

These cell-type-specific effects, together with the ability of Aβ to alter neuronal cytoskeletal organization and mechanics, prompted us to investigate the relationship between Aβ42 oligomers and Piezo1. Measurements of cellular Young's modulus, F-actin morphology, intracellular Ca^{2+} levels, and cell viability were performed in differentiated SH-SY5Y cells following exposure to Aβ42 oligomers.

2. Materials and methods

2.1. Cell culture and differentiation

SH-SY5Y cells were purchased from Wuhan Procell Life Technology Co., Ltd. (catalogue no. CL-0208). SH-SY5Y cells were cultured and differentiated using media adapted from published protocols [18–20] and optimized for local laboratory conditions. Detailed culture and differentiation procedures are provided in Supplementary Information.

2.2. AFM measurement and analysis of Young's modulus

Cellular mechanical properties were measured with an atomic force microscope (MFP-3D, Oxford Instruments) using an MSCT cantilever (probe D; Bruker). As the probe approached and indented the cell surface under piezoelectric control, cantilever deflection altered the angle of the reflected laser beam detected by the photodiode. The resulting force-indentation curves were used to calculate Young's modulus (Fig. 1a).

Before each experiment, probes were immersed for 60 min in 2 mL of piranha solution (1.5 mL of 98% H_2SO_4 and 0.5 mL of 30% H_2O_2), rinsed sequentially with ultrapure water and ethanol, exposed to ozone for 20 min, and dried in a desiccator for 2 h [21].

Young's modulus describes a material's resistance to elastic deformation. Cells were treated as soft materials, and force-indentation data were fitted using the stated contact-mechanics model [22, 23]:

$$\mathrm{F} = \frac{4}{3} \times \frac{E}{(1 - \nu^2)} \times \sqrt{R} \cdot \delta^{1.5}$$

In the model, F denotes loading force, E Young's modulus, v Poisson's ratio, R probe radius, and δ the probe-tip half angle. The parameters used were v = 0.5 [22, 23], R = 10 nm, and δ = 36°.

To determine how Aβ42 oligomers affect neuronal mechanics, Young's modulus was measured in differentiated SH-SY5Y cells by AFM. To reduce bias from spatial heterogeneity, all indentations were acquired over thick perinuclear regions (Fig. S1e). Force-indentation curves were processed in AtomicJ [24]. Only fits with $R^2 \geq 0.98$ were retained for Gaussian fitting and calculation of Young's modulus.

2.3. Western blot image presentation

Western blot procedures are described in the Supplementary Information. PVDF membranes were kept intact and were not trimmed before blocking or antibody incubation. Enhanced chemiluminescence (ECL) substrate was applied locally to the target-band regions to conserve reagent. Protein-band regions were cropped for presentation in Figs. 2b,d, 4c and 5c and Fig. S1a; black borders and white space delineate the displayed crops. Source chemiluminescence images and corresponding bright-field membrane photographs are provided in the Supplementary Information. The original GAPDH chemiluminescence file for Fig. 2d was lost because of a historical storage error; a photograph of the archived membrane is included. Caspase-1 in Fig. 5c was measured on a separate membrane without a loading control, and the analysis in Fig. 5d used unnormalized band gray values.

3. Results and discussion

3.1. Aβ42 oligomers induce rapid elevation of Young's modulus in SH-SY5Y cells

Firstly, the temporal relationship between Aβ42 oligomer exposure and cellular mechanics was characterized through the Young's modulus measurement repeatedly in differentiated SH-SY5Y cells by AFM (Fig. 1a). Following treatment with 1 μg/mL Aβ42 oligomers, stiffness increased from approximately 5 to 10 kPa over the first 3 h, remained near 10 kPa for approximately 3 h, and subsequently declined rapidly below baseline over the next 2 h (Fig. 1b). To compare baseline stiffness with the plateau phase, cells were treated with 1 μg/mL Aβ42 oligomers for 3 h and force curves were collected during the subsequent hour. Mean Young's modulus increased from 3.20 ± 0.84 kPa in control cells (Fig. 1c) to 9.93 ± 1.21 kPa after Aβ42 oligomer treatment (Fig. 1f), demonstrating a marked early increase in cellular stiffness.

Given the sensitivity of Piezo1 activity to membrane mechanics [25], the effect of pharmacological modulation of Piezo1 on the stiffness response was subsequently investigated. Treatment with 1 μM Yoda1, a Piezo1 agonist, for 5 h produced a modest increase in Young's modulus (4.65 ± 0.89 kPa; Fig. 1d), whereas 1 μM GsMTx4 reduced stiffness to 2.51 ± 0.53 kPa (Fig. 1e), approximately 22% below the control value. When cells were pretreated for 2 h and subsequently exposed to 1 μg/mL Aβ42 oligomers for an additional 3 h, Young's modulus reached 13.25 ± 1.55 kPa in the Yoda1 group (Fig. 1g) and 10.44 ± 2.15 kPa in the GsMTx4 group (Fig. 1h). Thus, Piezo1 modulation influenced the mechanical response, but GsMTx4 did not abolish the Aβ42-induced increase in stiffness. These findings suggest

that Aβ42-driven cytoskeletal remodeling establishes a mechanical state that may facilitate aberrant Piezo1 activity rather than being explained by Piezo1 alone.

Figure 1 Young's modulus of differentiated SH-SY5Y cells under different conditions. (a) Schematic of AFM-based measurement of cellular Young's modulus. (b) Time course after treatment with 1 μg/mL Aβ42 oligomers; 500 valid force curves were collected per time point across nine hourly measurements, and shading indicates the 95% confidence interval. (c–h) Distributions of Young's modulus after the indicated treatments; 3000–7000 valid force curves from 20–40 cells were analyzed per condition: (c) control; (d) 1 μM Yoda1 for 5 h; (e) 1 μM GsMTx4 for 5 h; (f) 1 μg/mL Aβ42 oligomers for 3 h; (g) Yoda1 pretreatment followed by Aβ42 oligomers; and (h) GsMTx4 pretreatment followed by Aβ42 oligomers. (i) Comparison of Young's modulus across the conditions mentioned above. Data are shown as mean ± SD and were analyzed by one-way ANOVA.

3.2. Aβ42 oligomers activate Piezo1-YAP/TAZ signaling and remodel F-actin

Immunofluorescence microscopy showed overlapping Piezo1 and Aβ42 signals in differentiated SH-SY5Y cells (Fig. 2a). Subsequently, reciprocal co-immunoprecipitation (co-IP) was performed to verify the presence of the proteins within the same complex.

Detection of both Piezo1 and Aβ42 was confirmed in input lysates, whereas no corresponding signal was observed in the IgG negative control. Piezo1 was recovered via immunoprecipitation with an anti-Aβ42 antibody, and Aβ42 was correspondingly recovered through reciprocal immunoprecipitation with an anti-Piezo1 antibody (Fig. 2b). These results support an intracellular association between Aβ42 oligomers and Piezo1, although they do not by themselves establish direct molecular binding.

Subsequently, Young's modulus was monitored at 30-minute intervals in both control and Piezo1-knockdown (Piezo1-KD) SH-SY5Y cells upon exposure to Aβ42 oligomers. In control cells, an increase in stiffness was observed during the first 3 h, followed by a plateau phase and a subsequent decline to below baseline levels by 6 h, accompanied by cell rounding and the development of overt death-associated morphology. Piezo1-KD cells also stiffened during the first 3 h, but the elevated Young's modulus persisted for longer; even after 9 h, the abrupt decline and death phenotype were not evident (Fig. 2c). Our previous research showed that mechanically activated Piezo1 promotes YAP nuclear translocation through Ca^{2+} influx [26–28]. Consistent with pathway activation, Aβ42 oligomer treatment reduced the phosphorylated-to-total YAP/TAZ ratio (Fig. 2d,e). Given the close association between YAP/TAZ signaling and cytoskeletal remodeling [29, 30], F-actin organization was examined (Fig. 2f). Control cells displayed stress fibers along differentiated neurite-like processes and fine microfilaments in the cell body. After Aβ42 oligomer exposure, neurite-like processes shortened by 3 h, F-actin became denser, and prominent microfilament clusters formed by 6 h. Together, these findings link the Aβ42-Piezo1 association to YAP/TAZ activation, F-actin remodeling, and time-dependent changes in cellular stiffness. The data support association and pathway involvement, but additional biophysical experiments are required to establish direct binding.

Figure 2 Aβ42 oligomers associate with Piezo1 and activate YAP/TAZ signaling. (a) Colocalization of Aβ42 and Piezo1 by confocal immunofluorescence microscopy; nuclei were labeled with DAPI. (b) Reciprocal Co-IP and immunoblot analysis. (c) Time-dependent changes in Young's modulus after exposure to 1 μg/mL Aβ42 oligomers in control and Piezo1-knockdown cells. (d,e) Immunoblot and quantitative analysis of total and phosphorylated YAP/TAZ after 4 h of Aβ42 oligomer treatment. (f) Time-dependent F-actin remodeling after treatment with 1 μg/mL Aβ42 oligomers; nuclei were labeled with DAPI and F-actin with FITC-phalloidin. Data are shown as mean ± SD and were analyzed by one-way ANOVA. In (b), the two protein rows are cropped from separate Co-IP membranes. For both rows, the sample lanes are, from left to right, input, IgG control, anti-Aβ immunoprecipitation and anti-Piezo1 immunoprecipitation; the upper row shows Piezo1 and the lower row shows Aβ. In (d), the protein rows are cropped from the corresponding target-protein images of the same membrane. Black borders and intervening white space delineate the crops. Source images and membrane photographs are included under “Source blots for Fig. 2b” and “Source blots for Fig. 2d” in the Supplementary Information. The original GAPDH chemiluminescence file for (d) is unavailable because of a historical storage error; an archived-membrane photograph is provided.

3.3. Aβ42 oligomers open Piezo1 channels and induce sustained intracellular Ca^{2+} overload

Given the role of Ca^{2+} as a major second messenger and the principal cation conducted by Piezo1, intracellular Ca^{2+} levels were monitored following exposure to Aβ42 oligomers (Fig. 3a). Aβ42 oligomers produced an oscillatory increase in intracellular Ca^{2+}. Yoda1 modestly enhanced this response, whereas GsMTx4 attenuated it. In control cells, GsMTx4 alone had little effect, while Yoda1 slightly increased Ca^{2+}, consistent with its agonist activity. Measurement of cell viability was subsequently performed using the Cell Counting Kit-8 (CCK-8) assay. At both 0.2 μg/mL (Fig. 3b) and 1 μg/mL (Fig. 3c) Aβ42 oligomers, Yoda1 increased cytotoxicity and GsMTx4 reduced it; neither modulator alone accounted for the loss of viability. Piezo1 knockdown further increased viability under both Aβ42 concentrations relative to non-knockdown controls (Fig. 3d). After 24 h of Aβ42 oligomer exposure, differentiated cells lost neurite-like processes and adopted a rounded, aggregated morphology (Fig. 3e). Pharmacological modulation and genetic knockdown therefore converge on a role for Piezo1 in Aβ42-induced Ca^{2+} dysregulation and cytotoxicity. Sustained Ca^{2+} imbalance may subsequently promote mitochondrial dysfunction, oxidative stress, and cell-death signaling.

Figure 3 Intracellular Ca^{2+} dynamics and cell viability following Aβ42 oligomer exposure and Piezo1 modulation. (a) Intracellular Ca^{2+} was monitored with Fluo-4 AM and confocal microscopy; fluorescence intensity was normalized to the initial value. (b,c) Time-dependent viability of SH-SY5Y cells treated with 0.2 μg/mL (b) or 1 μg/mL (c) Aβ42 oligomers. (d) Viability of control and Piezo1-knockdown cells exposed to different Aβ42 oligomer concentrations. (e) Morphological changes after treatment with 1 μg/mL Aβ42 oligomers for 24 h.

3.4. Aβ42 oligomer-mediated Ca^{2+} influx triggers mitochondrial damage and oxidative stress

Sustained cytosolic Ca^{2+} elevation can cause mitochondrial calcium overload, swelling, cristae disruption, and loss of mitochondrial membrane potential [31, 32]. Assessment of mitochondrial membrane potential (Δψm) was performed using JC-1. Red fluorescence indicates high Δψm, whereas green fluorescence indicates depolarized or damaged mitochondria. Control, Yoda1-only, and GsMTx4-only groups retained high Δψm. Aβ42 oligomer treatment decreased Δψm; Yoda1 intensified this effect, whereas GsMTx4 attenuated it (Fig. 4a). Given the capacity of mitochondrial dysfunction to elevate oxidative stress, intracellular ROS levels were additionally quantified (Fig. 4b). ROS remained low in the control and single-agent groups, increased after Aβ42 oligomer treatment, increased further with Yoda1, and was reduced by GsMTx4. These parallel changes implicate Piezo1-dependent Ca^{2+} signaling in Aβ42-associated mitochondrial dysfunction and ROS accumulation.

Ca^{2+}/calmodulin-dependent protein kinase IIα (CaMKIIα) regulates synaptic plasticity, learning, and memory, and Thr286 autophosphorylation is required for sustained activation [33]. Excessive CaMKIIα activity can promote tau phosphorylation and aggregation [34, 35], while disruption of the CaMKIIα-Ca^{2+}/calmodulin complex has been linked to calcium dyshomeostasis in Parkinson's disease [36]. To examine the contribution of CaMKIIα to Aβ42-induced injury, cells were treated with the CaMKII inhibitor KN93 and viability was measured by CCK-8 assay. KN93 significantly improved viability after Aβ42 oligomer exposure (Fig. 4e), supporting a role for CaMKII signaling downstream of Ca^{2+} dysregulation. Together, these results connect the Piezo1-Ca^{2+} axis with mitochondrial injury, oxidative stress, and CaMKII-dependent signaling, although direct pathway ordering will require additional intervention experiments.

Figure 4 Downstream effects of Aβ42 oligomer-induced Ca^{2+} influx. (a) Mitochondrial membrane potential measured with JC-1. (b) Relative cytosolic ROS levels across treatment groups. (c,d) Immunoblot and quantitative analysis of CaMKIIα and p-CaMKIIα. (e) Effect of the CaMKII inhibitor KN93 on viability after exposure to different concentrations of Aβ42 oligomers. Data are shown as mean ± SD and were analyzed by one-way ANOVA. In (c), the protein rows are cropped from the corresponding target-protein images of the same membrane and separated by black borders and white space. Source chemiluminescence images and membrane photographs are included under “Source blots for Fig. 4c” in the Supplementary Information.

3.5. Aβ42 oligomers trigger SH-SY5Y cell death through the non-canonical pyroptosis pathway

Aβ42 oligomer-treated SH-SY5Y cells displayed swelling and rounding (Fig. 2f), prompting us to investigate the mode of cell death. Pyroptosis disrupts the plasma membrane and releases lactate dehydrogenase (LDH) into the culture supernatant. Aβ42 oligomers increased LDH release in a

concentration-dependent manner (Fig. 5b). Immunoblot analysis further showed an approximately fourfold increase in the N-terminal fragment of gasdermin D (GSDMD-N), the pore-forming domain of GSDMD (Fig. 5c,d). Unnormalized caspase-1 band gray values did not differ significantly between groups, whereas caspase-4 increased approximately threefold after Aβ42 oligomer treatment. Because caspase-1 was measured without a loading control, this comparison does not establish unchanged normalized caspase-1 abundance. Together with caspase-4 immunofluorescence (Fig. 5a), these findings are consistent with activation of caspase-4-mediated non-canonical pyroptosis. Functional inhibition or genetic rescue experiments will be needed to establish whether this pathway is necessary for Aβ42-induced cell death.

Figure 5 Aβ42 oligomers induce pyroptosis-associated changes in SH-SY5Y cells. (a) Caspase-4 immunofluorescence. (b) LDH release after 24 h of treatment with different concentrations of Aβ42 oligomers. (c,d) Immunoblot and quantitative analysis of pyroptosis-related proteins. Data are shown as mean ± SD and were analyzed by one-way ANOVA. For the caspase-1 statistical analysis presented in Fig. 5d, quantification was performed directly using the raw gray value of the target bands without normalization to a loading control. In (c), the GSDMD, caspase-4, GAPDH and N-GSDMD rows originate from one membrane; the caspase-1 row originates from a separate membrane. The GAPDH row is associated with the caspase-4 pathway membrane and is not a loading control for caspase-1. Black borders and white space delineate the cropped protein rows. Source images and photographs of both membranes are included under “Source blots for Fig. 5c” in the Supplementary Information.

4. Conclusions

This study shows that Aβ42 oligomers associate with Piezo1 and promote sustained Ca^{2+} influx in differentiated SH-SY5Y cells. Piezo1-dependent calcium dysregulation was accompanied by cytoskeletal remodeling, altered cellular stiffness, mitochondrial dysfunction, ROS accumulation, and molecular features consistent with caspase-4-mediated non-canonical pyroptosis. These results identify a mechanochemical pathway that may contribute to Aβ42 neurotoxicity and warrant further investigation of Piezo1 in AD models.

Learning and memory depend on stable neuronal membrane potential and tightly regulated ion channel activity. Chronic Aβ42-associated Piezo1 activation could disrupt membrane potential, intracellular Ca^{2+} homeostasis, and redox balance, thereby impairing neuronal function over time. The present findings therefore provide a testable mechanistic framework linking altered cellular mechanics to progressive neuronal dysfunction in AD.

This study has several limitations. All experiments used the SH-SY5Y neuroblastoma cell line rather than primary neurons, and the *in vitro* system does not reproduce the multicellular and mechanical complexity of the brain. The study also does not resolve cell-type-specific Piezo1 responses or establish direct molecular binding between Aβ42 and Piezo1. Future work should validate the pathway in primary neurons, brain organoids, and animal models; define the molecular basis of the Aβ42-Piezo1 association;

and test whether Piezo1 or downstream Ca^{2+} signaling can be modulated without impairing protective Piezo1 functions in other neural cell types.

Declarations

Funding

This work was financially supported by the National Key R&D Program of China (Nos. 2024YFA1307400 and 2022YFF0712504 to H.W.), National Key R&D Program of China, Project on Intergovernmental International Science and Technology Innovation Cooperation (2026YFE0104200), National Natural Science Foundation of China (No. 22327808, 22595380, 22595381 to H.W., No. 22277116 to Y.S.).

Competing interests

The authors declare that they have no known competing financial interests or personal relationships that could have appeared to influence the work reported in this paper.

Author contributions

Weiqi Meng: writing – original draft, investigation, formal analysis, visualization.

Junye Zhang and Shuming Zhang: instrumental guidance.

Yan Shi and Hongda Wang: writing – review and editing, resources, conceptualization, funding acquisition.

All authors read and approved the final manuscript.

Data availability

Data will be made available on request.

References

1. van der Kant, R., Goldstein, L. S. B. & Ossenkoppele, R. Amyloid-β-independent regulators of tau pathology in Alzheimer disease. *Nat. Rev. Neurosci.* **21** (1), 21–35. https://doi.org/10.1038/s41583-019-0240-3 (2020).
2. Xie, L. et al. A multi-cohort study of longitudinal and cross-sectional Alzheimer's disease biomarkers in cognitively unimpaired older adults. *Alzheimers Dement.* **21** (2), e14492. https://doi.org/10.1002/alz.14492 (2025).
3. Kreutzer, A. G. et al. Antibodies raised against an Aβ oligomer mimic recognize pathological features in Alzheimer's disease and associated amyloid-disease brain tissue. *ACS Cent. Sci.* **10** (1), 104–121. https://doi.org/10.1021/acscentsci.3c00592 (2023).

4. Li, C., Wang, R., Zhang, Y., Hu, C. & Ma, Q. PIAS3 suppresses damage in an Alzheimer's disease cell model by inducing the STAT3-associated STAT3/Nestin/Nrf2/HO-1 pathway. *Mol. Med.* **27** (1), 150. https://doi.org/10.1186/s10020-021-00410-3 (2021).
5. Yang, X. et al. The piperine derivative HJ105 inhibits Aβ1–42-induced neuroinflammation and oxidative damage via the Keap1-Nrf2-TXNIP axis. *Phytomedicine* **87**, 153571. https://doi.org/10.1016/j.phymed.2021.153571 (2021).
6. Cai, Y. et al. DHPA protects SH-SY5Y cells from oxidative stress-induced apoptosis via mitochondria apoptosis and the Keap1/Nrf2/HO-1 signaling pathway. *Antioxid. (Basel)*. **11** (9), 1794. https://doi.org/10.3390/antiox11091794 (2022).
7. Ruiz-Reig, N. et al. KIF2A downregulation links amyloid-β to Tau phosphorylation in Alzheimer's disease. *Brain* **149** (5), 1650–1662. https://doi.org/10.1093/brain/awaf382 (2026).
8. Bettamin, L. et al. Real-time and high-resolution monitoring of neuronal electrical activity and pH variations based on the co-integration of nanoelectrodes and chem-FinFETs. *Small* **20** (27), e2309055. https://doi.org/10.1002/smll.202309055 (2024).
9. Li, D. et al. Nanomechanical profiling of Aβ42 oligomer-induced biological changes in single hippocampus neurons. *ACS Nano*. **17** (6), 5517–5527. https://doi.org/10.1021/acsnano.2c10861 (2023).
10. Wang, B. et al. Mechanosensitive ion channel Piezo1 activated by matrix stiffness regulates oxidative stress-induced senescence and apoptosis in human intervertebral disc degeneration. *Oxid. Med. Cell. Longev.* **2021**, 8884922. https://doi.org/10.1155/2021/8884922 (2021).
11. Chu, F. et al. Transcranial magneto-acoustic stimulation attenuates synaptic plasticity impairment through the activation of Piezo1 in Alzheimer's disease mouse model. *Res. (Wash D C)*. **6**, 0130. https://doi.org/10.34133/research.0130 (2023).
12. Lin, Y. C. et al. Force-induced conformational changes in PIEZO1. *Nature* **573** (7773), 230–234. https://doi.org/10.1038/s41586-019-1499-2 (2019).
13. Wang, H. J. et al. Microscale geometrical modulation of PIEZO1 mediated mechanosensing through cytoskeletal redistribution. *Nat. Commun.* **15** (1), 5521. https://doi.org/10.1038/s41467-024-49833-6 (2024).
14. Chi, S. et al. Astrocytic Piezo1-mediated mechanotransduction determines adult neurogenesis and cognitive functions. *Neuron* **110** (18), 2984–2999. https://doi.org/10.1016/j.neuron.2022.07.010 (2022).
15. Hu, J. et al. Microglial Piezo1 senses Aβ fibril stiffness to restrict Alzheimer's disease. *Neuron* **111** (1), 15–29. https://doi.org/10.1016/j.neuron.2022.10.021 (2023).
16. Jäntti, H. et al. Microglial amyloid beta clearance is driven by PIEZO1 channels. *J. Neuroinflammation*. **19** (1), 147. https://doi.org/10.1186/s12974-022-02486-y (2022).
17. Ke, W. et al. Matrix stiffness induces Drp1-mediated mitochondrial fission through Piezo1 mechanotransduction in human intervertebral disc degeneration. *J. Transl Med.* **21** (1), 711. https://doi.org/10.1186/s12967-023-04590-w (2023).

18. Shipley, M. M., Mangold, C. A. & Szpara, M. L. Differentiation of the SH-SY5Y human neuroblastoma cell line. *J. Vis. Exp.* **108**, 53193. https://doi.org/10.3791/53193 (2016).
19. Boban, M., Babić Leko, M., Miškić, T., Hof, P. R. & Šimić, G. Human neuroblastoma SH-SY5Y cells treated with okadaic acid express phosphorylated high molecular weight tau-immunoreactive protein species. *J. Neurosci. Methods*. **319**, 60–68. https://doi.org/10.1016/j.jneumeth.2018.09.030 (2019).
20. Zhang, T., Song, C., Zheng, C., Chen, X. & Zhang, Y. Extracellular amyloid β-protein (1–42) oligomers anchor brain cells and make them inert as an unconventional integrin-coupled ligand. *Cell. Mol. Neurobiol.* **43** (2), 841–858. https://doi.org/10.1007/s10571-022-01219-2 (2023).
21. Shan, Y. et al. The study of single anticancer peptides interacting with HeLa cell membranes by single molecule force spectroscopy. *Nanoscale* **4** (4), 1283–1286. https://doi.org/10.1039/c2nr11541g (2012).
22. Codan, B. et al. Exploring the elasticity and adhesion behavior of cardiac fibroblasts by atomic force microscopy indentation. *Mater. Sci. Eng. C*. **40**, 427–434. https://doi.org/10.1016/j.msec.2014.04.003 (2014).
23. Sneddon, I. N. The relation between load and penetration in the axisymmetric Boussinesq problem for a punch of arbitrary profile. *Int. J. Eng. Sci.* **3**, 47–57. https://doi.org/10.1016/0020-7225(65)90019-4 (1965).
24. Carl, P. & Schillers, H. Elasticity measurement of living cells with an atomic force microscope: data acquisition and processing. *Pflugers Arch.* **457** (2), 551–559. https://doi.org/10.1007/s00424-008-0524-3 (2008).
25. Xu, L. et al. PIEZO1 mediates periostin+ myofibroblast activation and pulmonary fibrosis in mice. *J. Clin. Invest.* **135** (11), e184158. https://doi.org/10.1172/jci184158 (2025).
26. Duan, J. et al. PIEZO1 affects cell growth and migration via microfilament-mediated YAP trans-latitudinal regulation. *Anal. Chem.* **97** (1), 147–156. https://doi.org/10.1021/acs.analchem.4c03420 (2025).
27. Liao, C. et al. Piezo1-mediated calcium flux transfers mechanosignal to Yes-associated protein to stimulate matrix production in keloid. *J. Invest. Dermatol.* **145** (11), 2869–2881. https://doi.org/10.1016/j.jid.2025.03.039 (2025).
28. Li, W. et al. PIEZO1-mediated calcium signaling and podocyte injury in diabetic kidney disease. *J. Am. Soc. Nephrol.* **36** (7), 1310–1326. https://doi.org/10.1681/asn.0000000634 (2025).
29. Scott, K. E., Fraley, S. I. & Rangamani, P. A spatial model of YAP/TAZ signaling reveals how stiffness, dimensionality, and shape contribute to emergent outcomes. *Proc. Natl. Acad. Sci. U S A*. **118** (20), e2021571118. https://doi.org/10.1073/pnas.2021571118 (2021).
30. Shen, Y. et al. Effects of vimentin intermediate filaments on the structure and dynamics of *in vitro* multicomponent interpenetrating cytoskeletal networks. *Phys. Rev. Lett.* **127** (10), 108101. https://doi.org/10.1103/physrevlett.127.108101 (2021).

31. Ramasinghe, L. P. et al. Influence of surface chemistry and nanomechanical properties of methacrylate-based copolymer thin films on keratocyte cell adhesion. *ACS Appl. Mater. Interfaces*. **17** (15), 23222–23236. https://doi.org/10.1021/acsami.4c21538 (2025).
32. Zmuda, M. et al. The *Bordetella* effector protein BteA induces host cell death by disruption of calcium homeostasis. *mBio* **15** (12), e01925–e01924. https://doi.org/10.1128/mbio.01925-24 (2024).
33. Sun, Y. et al. Inhibition of nuclear deacetylase Sirtuin-1 induces mitochondrial acetylation and calcium overload leading to cell death. *Redox Biol.* **53**, 102334. https://doi.org/10.1016/j.redox.2022.102334 (2022).
34. Moloney, C. M. et al. Phosphorylated tau sites that are elevated in Alzheimer's disease fluid biomarkers are visualized in early neurofibrillary tangle maturity levels in the post mortem brain. *Alzheimers Dement.* **19** (3), 1029–1040. https://doi.org/10.1002/alz.12749 (2023).
35. Chinnathambi, S. & Rangappa, N. SUMO inhibits Tau aggregation in Alzheimer's disease. *Adv. Protein Chem. Struct. Biol.* **147**, 355–374. https://doi.org/10.1016/bs.apcsb.2025.02.001 (2025).
36. Pullara, F. et al. NADPH oxidase 2 activity disrupts calmodulin/CaMKIIα complex via redox modifications of CaMKIIα-contained Cys30 and Cys289: implications in Parkinson's disease. *Redox Biol.* **75**, 103254. https://doi.org/10.1016/j.redox.2024.103254 (2024).
37. Liu, X., Zhang, J., Xu, H., Shao, L. & Wang, H. Dark-vacuole bodies studying by high-resolution label-free microscopy assisted with fluorescence technology. *Chem. Res. Chin. Univ.* **40** (6), 978–986. https://doi.org/10.1007/s40242-024-3271-x (2024).
38. Shao, L. et al. Label-free super-resolution microscopy for long-term monitoring the dynamic interactions of cellular organelles. *Chem. Res. Chin. Univ.* **40** (6), 994–1003. https://doi.org/10.1007/s40242-024-4006-8 (2024).

Figures

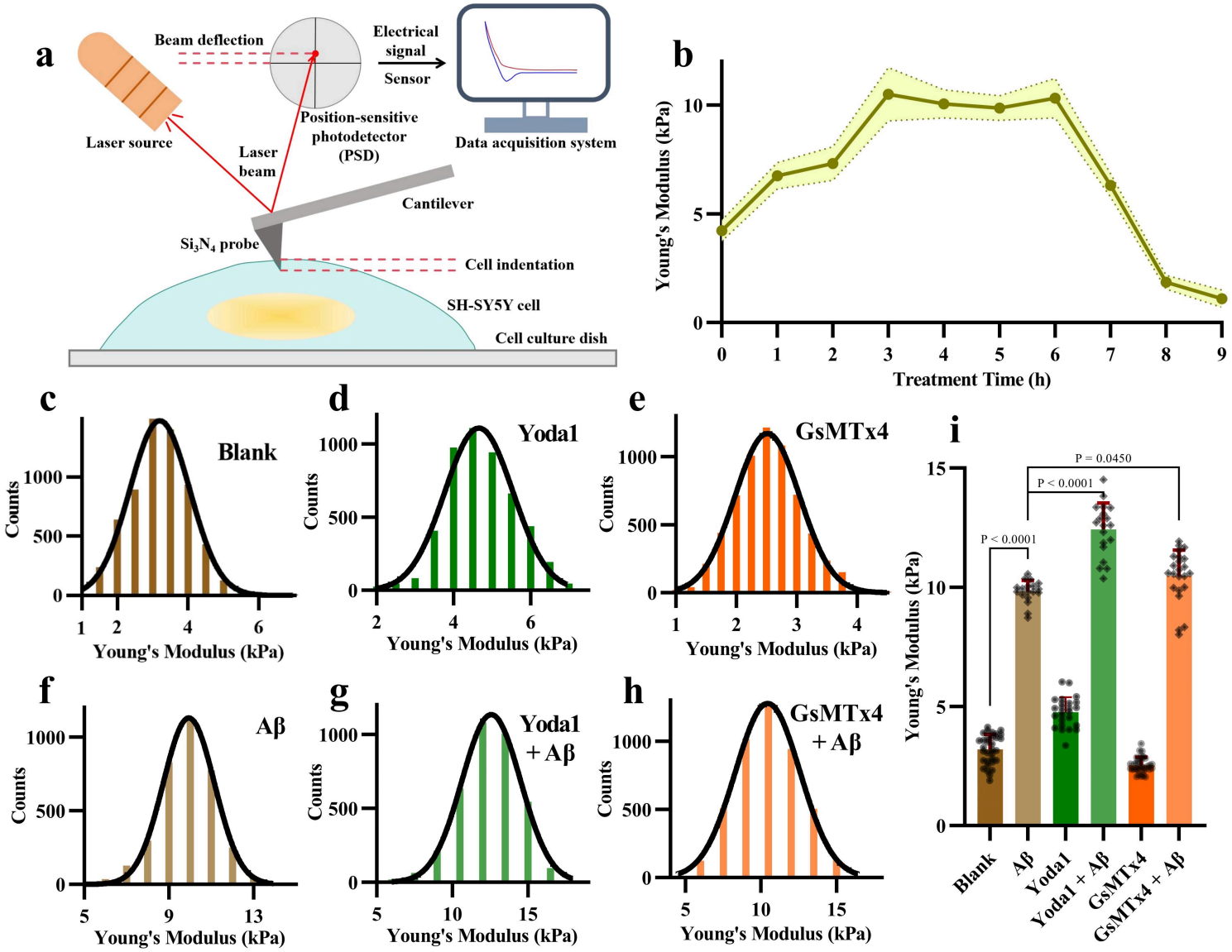


Figure 1

Young's modulus of differentiated SH-SY5Y cells under different conditions. (a) Schematic of AFM-based measurement of cellular Young's modulus. (b) Time course after treatment with 1 μg/mL Aβ42 oligomers; 500 valid force curves were collected per time point across nine hourly measurements, and shading indicates the 95% confidence interval. (c–h) Distributions of Young's modulus after the indicated treatments; 3000–7000 valid force curves from 20–40 cells were analyzed per condition: (c) control; (d) 1 μM Yoda1 for 5 h; (e) 1 μM GsMTx4 for 5 h; (f) 1 μg/mL Aβ42 oligomers for 3 h; (g) Yoda1 pretreatment followed by Aβ42 oligomers; and (h) GsMTx4 pretreatment followed by Aβ42 oligomers. (i) Comparison of Young's modulus across the conditions mentioned above. Data are shown as mean ± SD and were analyzed by one-way ANOVA.

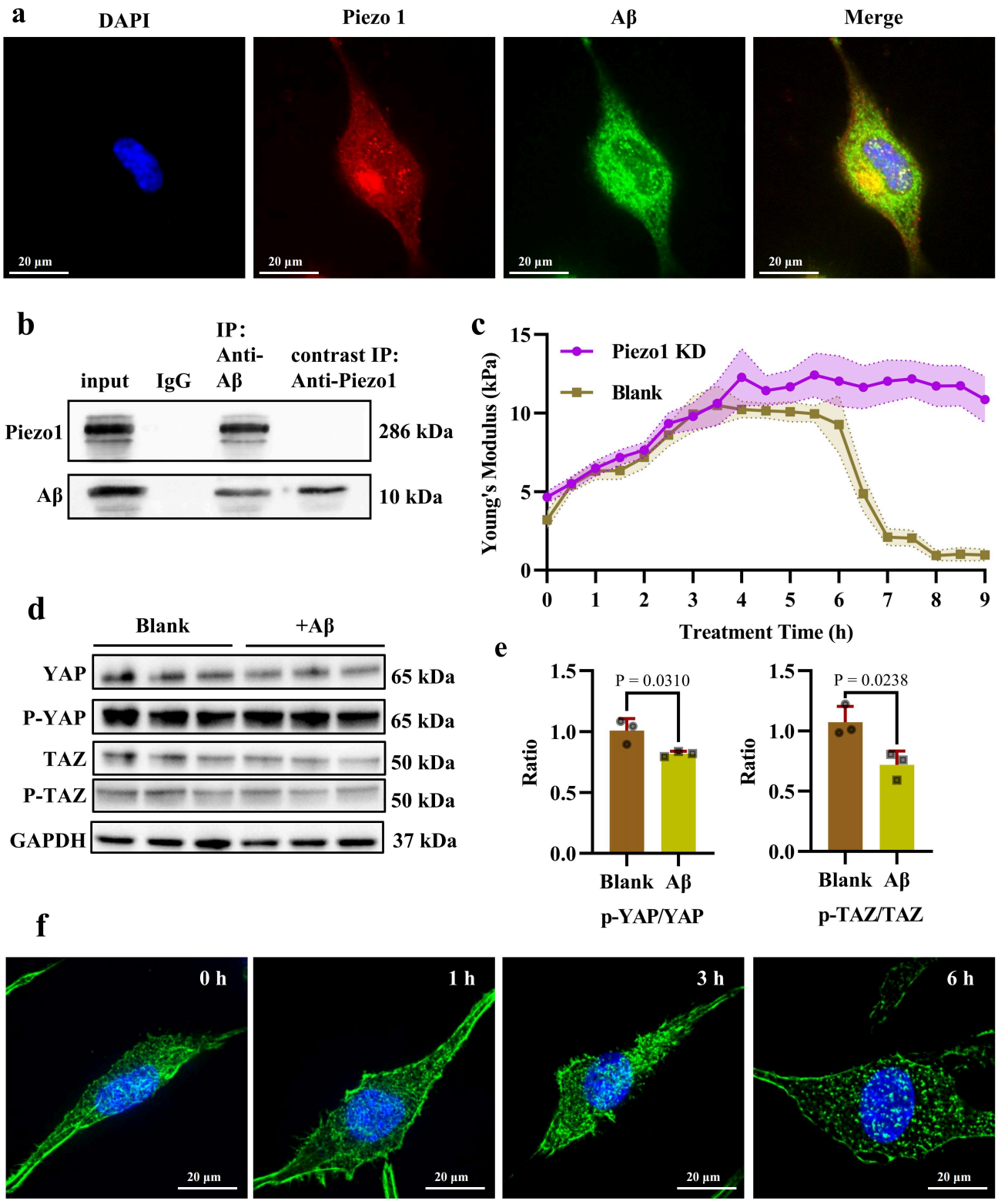


Figure 2

Aβ42 oligomers associate with Piezo1 and activate YAP/TAZ signaling. (a) Colocalization of Aβ42 and Piezo1 by confocal immunofluorescence microscopy; nuclei were labeled with DAPI. (b) Reciprocal Co-IP and immunoblot analysis. (c) Time-dependent changes in Young's modulus after exposure to 1 μg/mL Aβ42 oligomers in control and Piezo1-knockdown cells. (d,e) Immunoblot and quantitative analysis of total and phosphorylated YAP/TAZ after 4 h of Aβ42 oligomer treatment. (f) Time-dependent F-actin

remodeling after treatment with 1 μg/mL Aβ42 oligomers; nuclei were labeled with DAPI and F-actin with FITC-phalloidin. Data are shown as mean ± SD and were analyzed by one-way ANOVA. In (b), the two protein rows are cropped from separate Co-IP membranes. For both rows, the sample lanes are, from left to right, input, IgG control, anti-Aβ immunoprecipitation and anti-Piezo1 immunoprecipitation; the upper row shows Piezo1 and the lower row shows Aβ. In (d), the protein rows are cropped from the corresponding target-protein images of the same membrane. Black borders and intervening white space delineate the crops. Source images and membrane photographs are included under “Source blots for Fig. 2b” and “Source blots for Fig. 2d” in the Supplementary Information. The original GAPDH chemiluminescence file for (d) is unavailable because of a historical storage error; an archived-membrane photograph is provided.

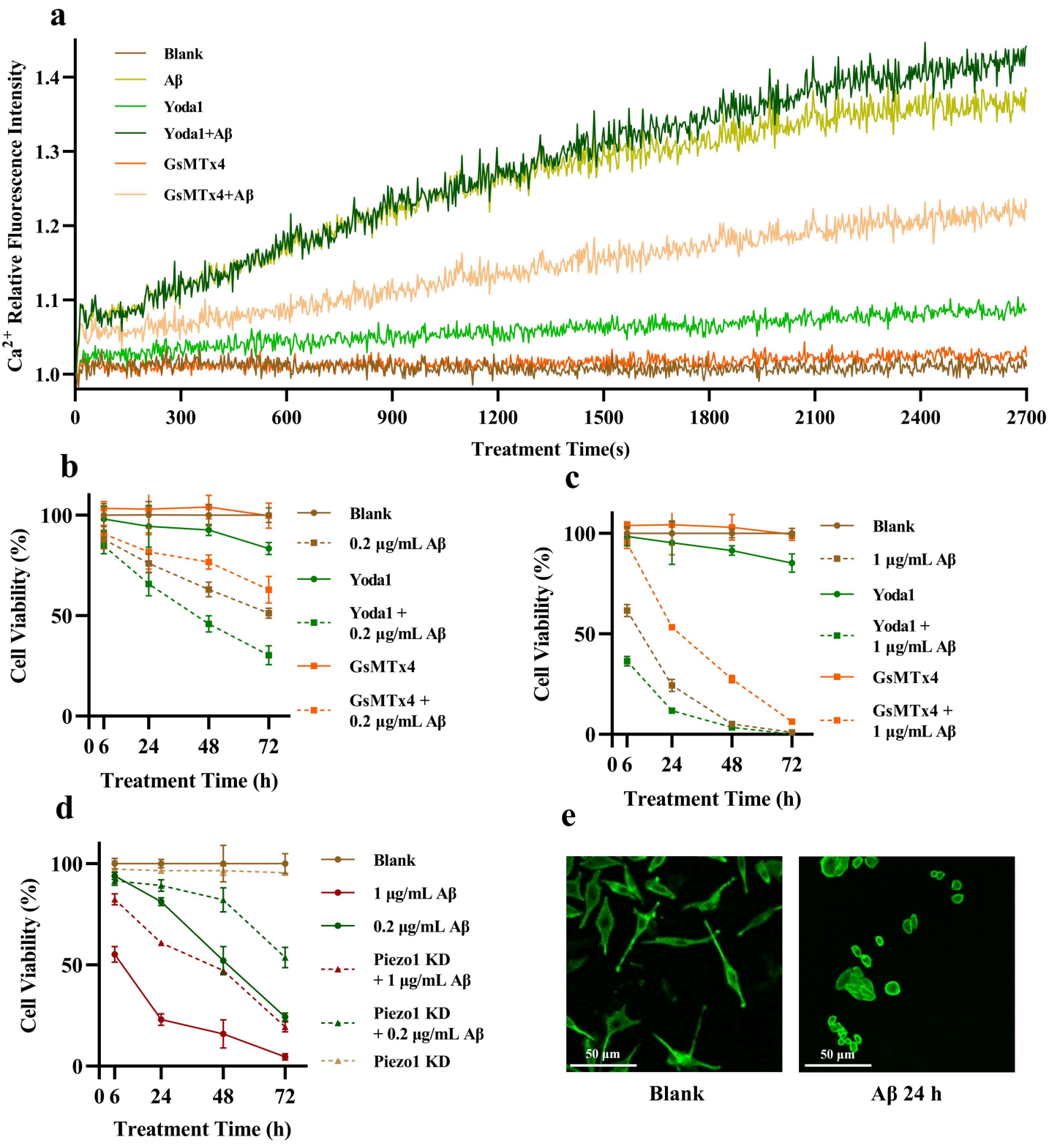


Figure 3

Intracellular Ca^{2+} dynamics and cell viability following Aβ42 oligomer exposure and Piezo1 modulation. (a) Intracellular Ca^{2+} was monitored with Fluo-4 AM and confocal microscopy; fluorescence intensity was normalized to the initial value. (b,c) Time-dependent viability of SH-SY5Y cells treated with 0.2 μg/mL (b) or 1 μg/mL (c) Aβ42 oligomers. (d) Viability of control and Piezo1-knockdown cells exposed

to different Aβ42 oligomer concentrations. (e) Morphological changes after treatment with 1 μg/mL Aβ42 oligomers for 24 h.

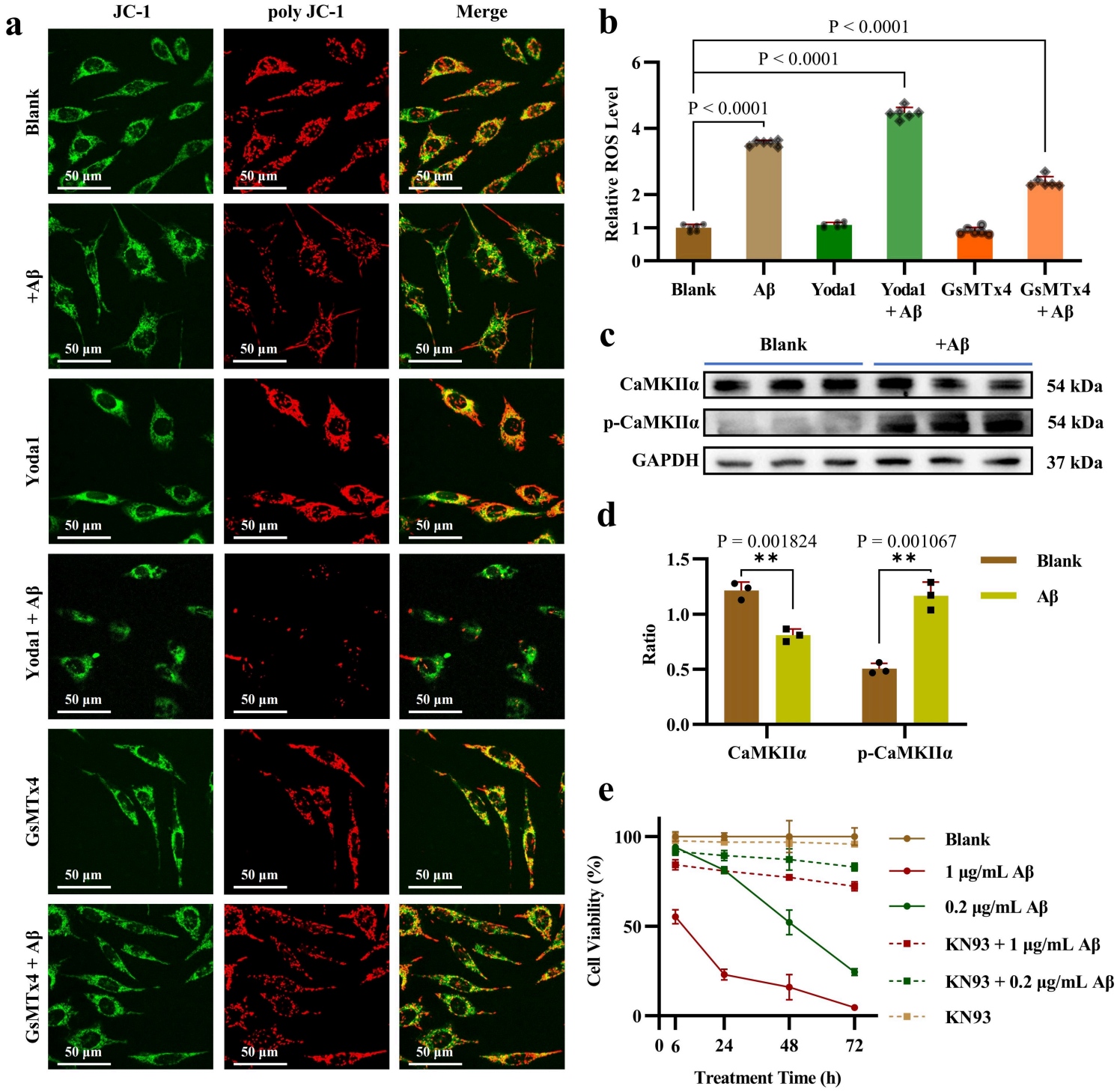


Figure 4

Downstream effects of Aβ42 oligomer-induced Ca^{2+} influx. (a) Mitochondrial membrane potential measured with JC-1. (b) Relative cytosolic ROS levels across treatment groups. (c,d) Immunoblot and quantitative analysis of CaMKIIα and p-CaMKIIα. (e) Effect of the CaMKII inhibitor KN93 on viability after exposure to different concentrations of Aβ42 oligomers. Data are shown as mean ± SD and were

analyzed by one-way ANOVA. In (c), the protein rows are cropped from the corresponding target-protein images of the same membrane and separated by black borders and white space. Source chemiluminescence images and membrane photographs are included under “Source blots for Fig. 4c” in the Supplementary Information.

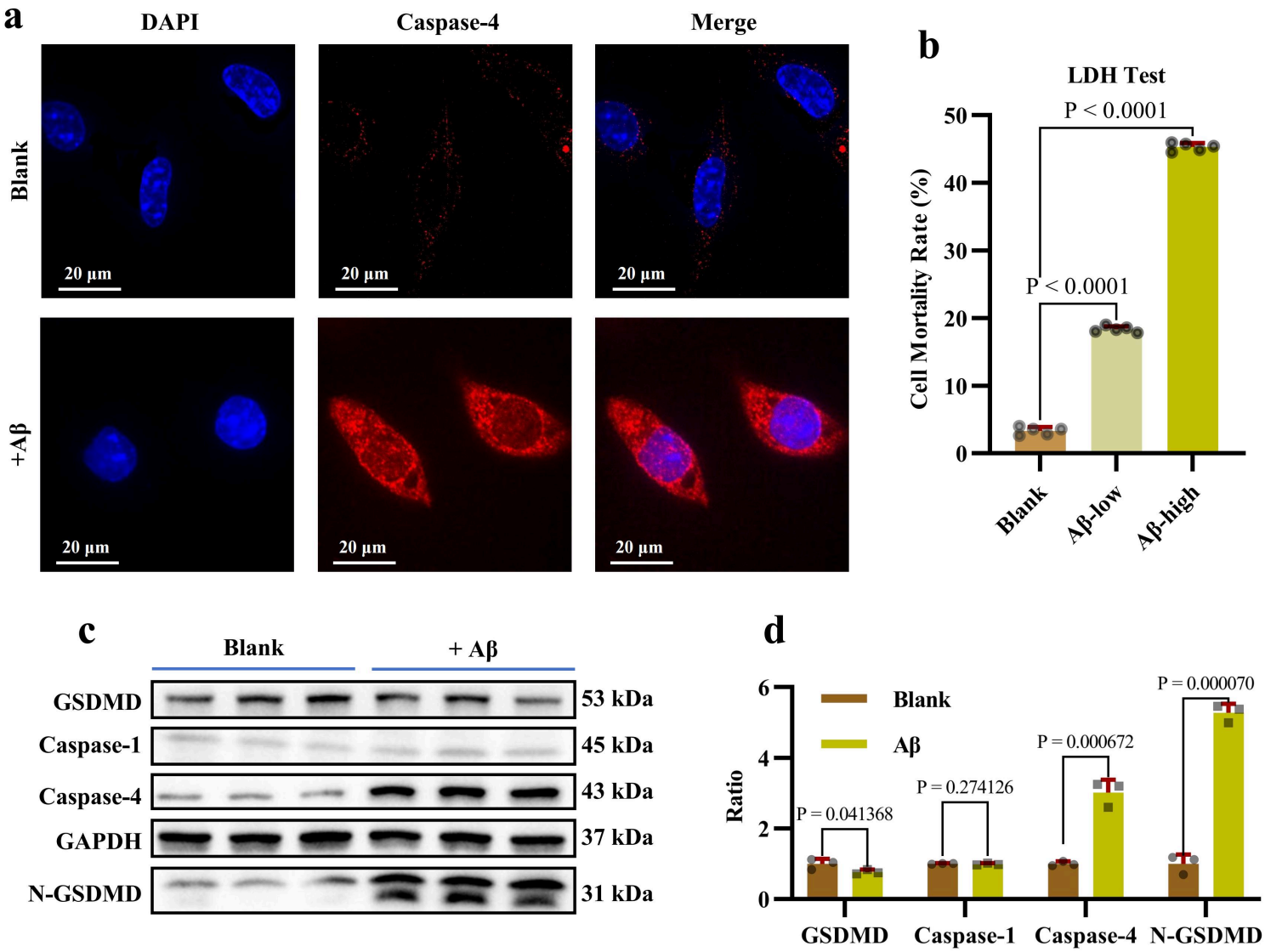


Figure 5

Aβ42 oligomers induce pyroptosis-associated changes in SH-SY5Y cells. (a) Caspase-4 immunofluorescence. (b) LDH release after 24 h of treatment with different concentrations of Aβ42 oligomers. (c,d) Immunoblot and quantitative analysis of pyroptosis-related proteins. Data are shown as mean ± SD and were analyzed by one-way ANOVA. For the caspase-1 statistical analysis presented in Figure 5d, quantification was performed directly using the raw gray value of the target bands without normalization to a loading control. In (c), the GSDMD, caspase-4, GAPDH and N-GSDMD rows originate from one membrane; the caspase-1 row originates from a separate membrane. The GAPDH row is associated with the caspase-4 pathway membrane and is not a loading control for caspase-1. Black

borders and white space delineate the cropped protein rows. Source images and photographs of both membranes are included under “Source blots for Fig. 5c” in the Supplementary Information.

Supplementary Files

This is a list of supplementary files associated with this preprint. Click to download.

- ScientificReportsSupplementaryInformation261008.pdf